PHOTONICS Research

Superior optical Kerr effects induced by two-dimensional excitons

Feng Zhou,[1,2] Cacere Jelah Nieva,[2] Dianyuan Fan,[1] Shunbin Lu,[1,3] and Wei Ji[1,2,4]

[1]SZU-NUS Collaborative Innovation Center for Optoelectronic Science & Technology, International Collaborative Laboratory of 2D Materials for Optoelectronic Science & Technology of Ministry of Education, Institute of Microscale Optoelectronics (IMO), Shenzhen University, Shenzhen 518060, China
[2]Department of Physics, National University of Singapore, Singapore 117542, Singapore
[3]e-mail: shunbin_lu@szu.edu.cn
[4]e-mail: phyjiwei@nus.edu.sg

Received 28 October 2021; revised 17 January 2022; accepted 24 January 2022; posted 25 January 2022 (Doc. ID 447029); published 1 March 2022

Materials with strong optical Kerr effects (OKEs) are crucial for a broad range of applications, such as all-optical data processing and quantum information. However, the underlying OKE mechanism is not clear in 2D materials. Here, we reveal key insights of the OKE associated with 2D excitons. An admirably succinct formalism is derived for predicting the spectra and the magnitude of the nonlinear refractive index (n_2) of 2D materials. The predicted n_2 spectra are consistent with reported experimental data and exhibit pronounced excitonic resonances, which is distinctively different from bulk semiconductors. The n_2 value is predicted to be 3×10^{-10} cm^2/W for a 2D layered perovskite at low temperature as 7 K, which is four orders of magnitude larger than those of bulk semiconductors. The superior OKE induced by 2D excitons would give rise to a narrow refractive index-near-zero region for intense laser light. Furthermore, we demonstrate that the 2D layered perovskite should exhibit the best OKE efficiency ($W_{\mathrm{FOM}} = 1.02$, $T_{\mathrm{FOM}} = 0.14$) at 1550 nm, meeting the material requirements for all-optical switching. Our findings deepen the understanding of the OKE of 2D semiconducting materials and pave the way for highly efficient all-optical excitonic devices.

https://doi.org/10.1364/PRJ.447029

1. INTRODUCTION

The optical Kerr effect (OKE) is one of the nonlinear optical (NLO) phenomena observed in dielectric or semiconducting materials, where the refractive index changes in response to intense laser light. The change of refractive index (or so-called nonlinear refractive index, n_2) leads to Kerr lensing [1] and phase modulation [2] of the laser light. By utilizing these characteristics, materials with the OKE have shown great potential for applications, such as all-optical switching, all-optical modulation, four wave mixing, optical parametric amplification, and laser mode-locking [3–8]. In the above-mentioned context, an ideal OKE material should possess large nonlinear refractive index at low optical power. In addition, a short response time is also crucial. Prior to this work, n_2 spectra of various 3D dielectrics and semiconductors have been experimentally measured [9–11] and theoretically verified via a two-parabolic band (TPB) model [12]. Such a theory provides a general guideline on predicting the n_2 magnitude of bulk semiconducting materials. However, 3D materials usually show either weak nonlinear refractive change or long response time even under illumination with strong optical fields. Such limitations therefore call for alternative strategies in order to obtain OKE materials for efficient all-optical devices.

One such strategy is to exploit excitonic effects of 2D materials (or so-called 2D excitons). The 2D exciton can be naturally formed by optical coupling excitonic transitions in layered materials where the spatial confinement and the reduced screening effect give rise to enhanced Coulomb interactions. Since the excitons are confined in a plane that is thinner than their Bohr radius in most 2D semiconductors [13–15], quantum confinement enhances the exciton binding energy [16] and alters materials' optical properties [17]. In particular, the 2D exciton layered materials manifest strong and ultrafast light–matter coupling on nonlinear optical responses in the visible to the near-infrared spectra [18,19]. For instance, a single crystal of Ruddlesden–Popper perovskite (RPP) in the 2D structure has been reported to possess an n_2 dispersion with a remarkable resonant feature arising from the Pauli blocking [1] in one-photon-induced transitions to the lowest excitonic state [20], giving rise to considerable OKEs in the visible range. The temporal response for this OKE has been reported to be ~100 ps, which is attributed to either an exciton-exciton

annihilation (EEA) effect or a radiative recombination process of the 1s excitons [21–24]. Apart from the one-photon absorption, OKEs along with the two-photon absorption (2PA) have also been reported in 2D semiconducting materials, where the photon energy ($\hbar\upsilon$) of the incident light is far below the bandgap (E_g), i.e., $E_g/2 < \hbar\upsilon < E_g$. It is noted that n_2 values of layered crystals of RPP, $(C_4H_9NH_3)_2(CH_3NH_3)_{n-1}Pb_nI_{3n+1}$ ($I_{n=1,2,3,4}$), have shown more than an order of magnitude, as compared with a bulk semiconductor and the TPB model [25] at the excitation wavelength of 2.7 μm. The enhancement of the OKEs was demonstrated to arise from excitonic effects on the 2PA [26,27]. Upon the 2PA associated OKEs, "dark" excitons are created instantaneously and then relax through electron-electron interaction, which exhibits a fast temporal decay <60 fs in transition metal dichalcogenide (TMD) monolayers and RPPs [23,27]. However, a theoretical guideline and systematic understanding on the OKE of 2D layered materials are still lacking.

In this paper, we develop a simple model on OKEs originated from 2D exciton-associated 2PA. By utilizing the second-order quantum perturbation theory for two-photon transitions among the energy states of 2D excitons and then performing the Kramers–Kronig (K-K) transformation, the nonlinear refractive index (n_2) is successfully derived over a broad range of light frequency with an assumption that only 2p exciton is taken into consideration. The theoretically calculated results from our model are comparable with those reported experimental data for monolayer RPPs, TMDs, black phosphorus (BP), and hexagonal boron nitrides (h-BNs). Furthermore, our model explicitly shows that the n_2 dispersions of 2D semiconductors are dominated by exciton-resonant features, in particular, the resonance with the 2p exciton; and the n_2 magnitudes are closely related to both its linewidth and energy level. The n_2 value of a 2D RPP is predicted to be 3×10^{-10} cm^2/W, which is four orders of magnitude more than those of bulk semiconductors ($\sim 10^{-14}$ cm^2/W) [10], demonstrating the superior OKEs induced by 2D excitons and implying a narrow refractive index-near-zero region for intense laser light. Last, we evaluate the figures-of-merit (FOMs) of the OKEs for these 2D semiconductors, which proves them to be of great potential for all-optical excitonic devices.

2. THEORY

The nonlinear refractive index (n_2) intrinsically accompanied by the 2PA coefficient (β) is governed by the K-K relation [1]. In the present context, we write it in the form

$$n_2(\hbar\upsilon) = \frac{c\hbar}{\pi}\int_0^{+\infty}\frac{\beta(\hbar\upsilon',\hbar\upsilon)\mathrm{d}(\hbar\upsilon')}{(\hbar\upsilon')^2-(\hbar\upsilon)^2}. \tag{1}$$

For a novel K-K transformation, two distinct photon energies for 2PA are needed, i.e., $\hbar\upsilon$ the "cause" and $\hbar\upsilon'$ the integration variable in Eq. (1). Here, we consider a special case for the degenerate 2PA, in which the photon energies $\hbar\upsilon$ and $\hbar\upsilon'$ are equivalent. The degenerate β in the case of exciton-resonant 2PA of 2D semiconductors is schematized by Fig. 1 and has been calculated based on a second-order, time-dependent, quantum-mechanical perturbation theory [28,29]. Here, we simplify the expression of degenerate β further, and the detailed

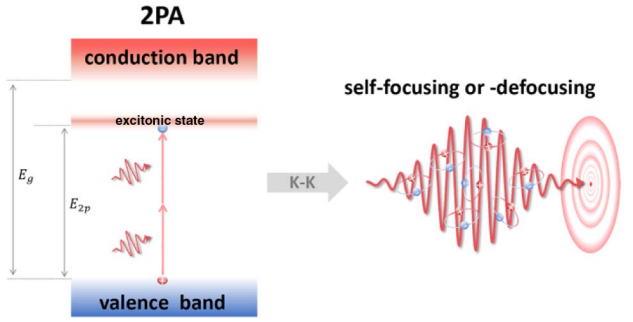

Fig. 1. Schematic of the optical Kerr effect (self-focusing or -defocusing) induced by 2PA resonant with the exciton energy (E_{2p}). E_g is the bandgap.

simplification can be found in the appendix. The simplified expression is as follows:

$$\beta(\hbar\upsilon') = C_2\frac{(n_0^2+2)^4}{E_{2p}^2}F_{2,\mathrm{exc}}(\hbar\upsilon'), \tag{2}$$

where C_2 is a material-related parameter (and its definition can be found in Appendix A); n_0 is the linear refractive index. $F_{2,\mathrm{exc}}(\hbar\upsilon') = \frac{\hbar\gamma}{(2\hbar\upsilon'-E_{2p})^2+(\hbar\gamma)^2}$ is the dispersion function with E_{2p} and $\hbar\gamma$ referring to the energy level of 2p excitonic state and half of its linewidth, respectively. Here, we assume that only 2p excitons make the contribution to the 2PA, and other excitonic states are ignored completely (see Fig. 1).

By substituting Eq. (2) into Eq. (1), the n_2 dispersion is derived to be

$$n_2(\hbar\upsilon) \approx \frac{c\hbar C_2}{\pi}\frac{(n_0^2+2)^4}{E_{2p}^2} \times \int_0^{E_{2p}}\frac{1}{(E_{2p}-2\hbar\upsilon')^2+(\hbar\gamma)^2}\frac{\hbar\upsilon'}{(\hbar\upsilon')^2-(\hbar\upsilon)^2}\mathrm{d}(\hbar\upsilon'). \tag{3}$$

Because the equivalence of $\hbar\upsilon$ and $\hbar\upsilon'$ would lead to the integral of $\beta(\hbar\upsilon')$ with divergences, a substitution of υ' with $\upsilon'+\Delta\upsilon'$ and a numerical summation were made for an approximate integral of β over the 2PA range ($0 < \hbar\upsilon' < E_{2p}$). With further simplifications, see the details in Appendix B; we obtain a semiempirical expression as

$$n_2(\hbar\upsilon) = \frac{Z_2'(n_0^2+2)^4}{E_{2p}^2}G(x), \tag{4}$$

where Z_2' is another material-related parameter, which is determined by the density (D_e), the effective Bohr radius (a_B), and the linewidth ($2\hbar\gamma$) of 2D excitons [24]. The definition of Z_2' can be found in Appendix A. The 10 2D materials (see Appendix C) have an average Z_2' value of 1×10^{-14} in the SI units such that n_2 is in cm^2/W, and $\hbar\upsilon$, E_{2p}, and $\hbar\gamma$ are in units of eV. $G(x)$ is given by

$$G(x) = \frac{0.5-x}{(0.5-x)^2+0.3(\hbar\gamma/E_{2p})^2}, \tag{5}$$

where $x = \hbar\upsilon/E_{2p}$.

3. RESULTS AND DISCUSSION

Note that Eq. (5) interprets the normalized n_2-dispersion. As shown by the pink area in Fig. 2, the normalized n_2 values with $\hbar\gamma/E_{2p}$ being in the range from 0.05 to 0.15 exhibit a central-symmetrical dispersion with respect to $x = 0.5$. For $|x - 0.5| \le 0.25$, the normalized n_2 values vary from the positive to the negative dramatically, indicating that the OKE would be on (or near) resonance with E_{2p}. Otherwise, the normalized n_2 values can be regarded as the off-resonant ones and are nearly independent on x or $\hbar\gamma/E_{2p}$.

To validate our model, the calculated n_2 dispersions are normalized and compared with experimental data of monolayer (or few-layer) TMDs, RPPs, h-BN, and BP [25,30–34], where the values of $E_{2p}^2/[Z_2'(n_0^2+2)^4]$ are obtained from Table 3 in Appendix A. In the off-resonance region, our model is in agreement with the experimental data within an order of magnitude for RPP ($I_{n=1}$) in polycrystalline structures (at 2.7 μm) [25] and h-BN (at 1.064 μm) [33]. The experimental data of RPP ($I_{n=2,3,4}$) powders are less than the prediction of Eq. (4). It is anticipated that surface states and/or surface scattering from the crystallites may hinder its intrinsic NLO properties of the 2D crystals. The normalized n_2 value of BP [34] is ~26 at $x = \hbar\upsilon/E_{2p} = 1.29$, which is comparable with the magnitude predicted by Eq. (4), but it is not shown because it is beyond the scale of the x axis in Fig. 2.

In the near-resonance region, there is a large discrepancy with the experimental data of monolayer (or few-layer) TMDs [30–32], which is attributed to the spin-split-off excitonic states. Experimental evidence has shown monolayer TMDs with the spin-orbital splitting possess a pair of generated excitons (as either the A-exciton or B-exciton [35]) transitioning at the K and K' valley in the momentum space with broken inversion symmetry. This gives rise to a unique valley degree of freedom in the n_2 dispersions that can directly couple to the helicity of excitation photons [17]. Under two-photon excitation, it is necessary to consider the two excitons; hence, as detailed in Appendix A, the n_2 dispersion is modified to be

$$n_2(\hbar\upsilon) = \frac{Z_2'(n_0^2+2)^4}{2E_{2p}^2}[G_A(x) + G_B(x)]. \quad (6)$$

Here, $E_{2p} = E_{2p\_A}$, $G_A(x) = \frac{0.5-x}{(0.5-x)^2+0.3(\hbar\gamma/E_{2p})^2}$, $G_B(x) = \frac{\Lambda\delta^2(1-0.5\delta-x)}{(1-0.5\delta-x)^2+0.3\delta^2(\Lambda\hbar\gamma/E_{2p})^2}$, $\delta = E_{2p\_A}/E_{2p\_B}$, $\hbar\gamma = \hbar\gamma_A$, and $\Lambda = \hbar\gamma_B/\hbar\gamma_A$.

Figure 3 shows good agreement between Eq. (6) and the experimental data. $G_A(x)$ and $G_B(x)$ result in two peaks in the near-resonance region, indicating that the spin-split-off energy of excitons should play a significant role in the OKE of monolayer TMD materials. Furthermore, the B-exciton with a higher energy level from the spin-orbital splitting leads to a broadened and blueshift of the resonance of the individual n_2 dispersion, in comparing the blue curves to the red ones in Fig. 3. This is attributed to higher energy levels of B-excitons, which exhibit larger linewidths of NLO resonance. The spin-splitting effect makes a great variation of overall n_2 values as displayed by the purple curves.

Figure 4 compares calculated n_2 magnitudes from Eq. (4) or Eq. (6) with the TPB model. It is interesting to note that the maximal n_2 values by Eq. (4) or Eq. (6) are in the range from 1×10^{-12} to 1×10^{-10} cm^2/W, which are greater than the TPB

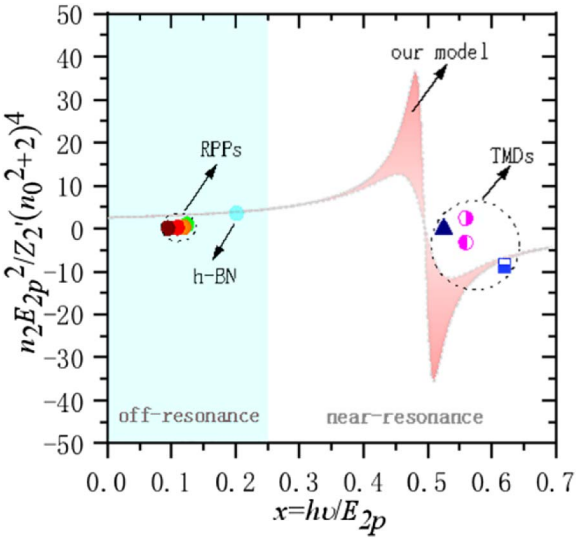

Fig. 2. Comparison of the normalized n_2 between the prediction (pink area) by Eq. (5) and the measured values (symbols) of monolayer (or few-layer) TMDs, RPP($I_{n=1}$), and h-BN [25,30–34]. The envelopes of the pink area are calculated with $\hbar\gamma/E_{2p} = 0.05$ and 0.15.

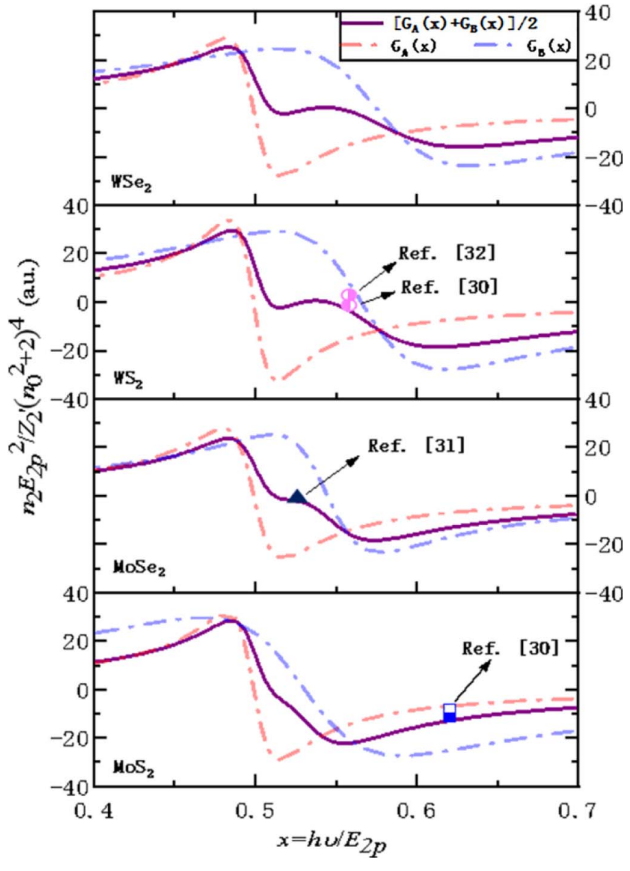

Fig. 3. Normalized n_2 dispersion of monolayer MoS_2, $MoSe_2$, WS_2, and WSe_2 calculated by the two excitons (purple), A exciton (red), and B exciton (blue) with $\hbar\gamma/E_{2p} = 0.075$ eV. The symbols are the experimental data from Refs. [30–32] and scaled with $Z_2' = 1 \times 10^{-14}$.

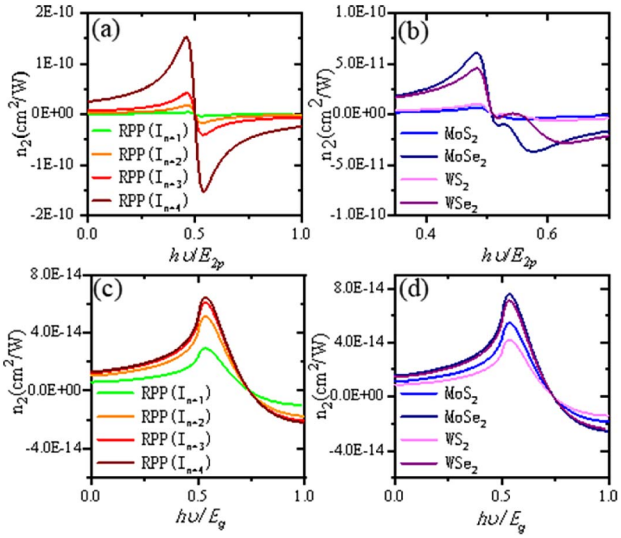

Fig. 4. Calculated n_2 dispersions of (a) monolayer RPP ($I_{n=1,2,3,4}$) and (b) TMDs by Eq. (4) and Eq. (6). Calculated n_2 dispersions of (c) monolayer RPP ($I_{n=1,2,3,4}$) and (d) TMDs by the two-parabolic-band model [12]. Parameters used in the calculation are displayed in Table 3 in Appendix A.

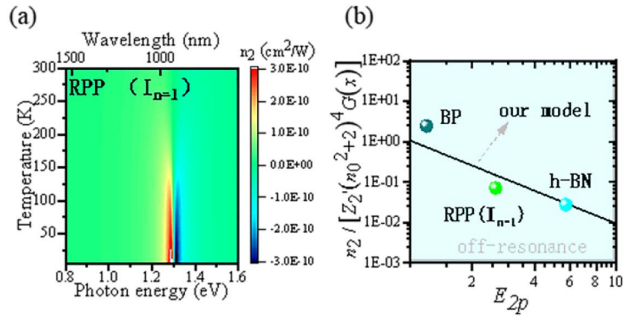

Fig. 5. (a) Calculated n_2 values as a function of photon energy (x axis) and temperature (y axis) for monolayer RPP ($I_{n=1}$). (b) A log-log plot of the scaled n_2 in the off-resonance region versus E_{2p}. The experimental n_2 values are scaled by $Z_2'(n_0^2+2)^4G(x)$ with n_0 and Z_2' listed in Table 3 in Appendix A. The solid line is the theoretical result of Eq. (4) with no adjustable parameters and a slope of −2.

model results by at least one order of magnitude. This indicates the 2D excitonic effects greatly enhance the OKE in 2D cases when compared with their bulk counterparts. As derived in Eqs. (4) and (6), the calculated n_2 values are proportional to $D_e \cdot a_B^4$, implying 2D materials possessing the higher density of excitons and/or the larger effective Bohr radius would exhibit greater OKE along with degenerate 2PA in many ways analogous to plasma screening effects [36]. As a result, RPP ($I_{n=4}$) is predicted to show the largest peak n_2 value of $\sim 1.5 \times 10^{-10}$ cm^2/W among the 10 materials. The calculated n_2 values are of the same order of magnitude as the multilayer graphene at an excitation wavelength in the near-infrared [37]. As compared with the experimental data of monolayer (or few-layer) TMDs in thin films, or dispersion [31,38–41], the measured absolute n_2 values are greater than from Eq. (6) [38,40,41]; also see Table 4 in Appendix C. One reason for the discrepancy is that the presence of a large number of defects/impurities in these films would give extra transitions in either 2PA or saturable absorption (SA) processes and, thus, enhance the measured nonlinearities. It is also noted that the absolute n_2 values from our model are one order of magnitude larger than the reported results of MoS_2 dispersion [31] and $MoSe_2$ nanosheets [39], where light scattering in those amorphous samples may screen a refractive index change arising from the 2D nature of excitons.

With the effects of 2D excitons, further enhancement of the OKE is predicted at lower temperature. As derived from Eq. (4) or (6), n_2 values on resonance are inversely proportional to the square of the linewidth ($2\hbar\gamma$) of 2D exciton, which would narrow down (as ∼35 meV) for RPPs, with temperature decreasing to ∼7 K [42]. The temperature dependence of the OKE could enlarge n_2 values at peak (or valley) by one order of magnitude [see an example of n_2 dispersion of RPP ($I_{n=1}$) in Fig. 5(a)]. The n_2 value of RPP ($I_{n=1}$) is predicted to be 3×10^{-10} cm^2/W at 7 K, which would lead to a change in the refractive index of 3 (i.e., around 150% of the linear refractive index) in the case of $I = 10$ GW/cm^2. This would give rise to a narrow refractive index-near-zero region of intense laser light when it is on resonance with 2D exciton. In the off-resonance region, our calculated n_2 values are nearly independent of $x = \hbar\upsilon/E_{2p}$ or the linewidth ($2\hbar\gamma$). The scaled n_2 values explicitly show an E_{2p}^{-2} dependence, which gives a variation by two orders of magnitude for 2D semiconducting materials with E_{2p} ranging from 1 to 10 eV. This variation is clearly illustrated in Fig. 5(b).

Indeed, in our model, the absolute magnitude of the nonlinear refractive index is enhanced through two-photon transitions, when the photon energy approaches $\hbar\upsilon/(2E_{2p})$. Such a resonant enhancement of n_2 is basically accompanied by absorption losses, commonly given by $\alpha = \alpha_0 + \beta I$, where α_0 is the linear absorption coefficient. The OKE efficiency/transparency trade-off (n_2/α) at a specific wavelength λ is therefore of importance to the assessment of a material for all-optical switching devices. The material requirements are as follows: $W_{\mathrm{FOM}} = \frac{|n_2|I}{\alpha_0\lambda} \gg 1$ and $T_{\mathrm{FOM}} = \frac{\beta\lambda}{|n_2|} \ll 1$ [43,44]. Table 1 lists the FOMs for selected materials operated at room temperature, $\lambda = 1550$ nm, and $I = 10$ GW/cm^2. Among them, RPP ($I_{n=4}$) is the best: its n_2 is predicted to be as large as 1×10^{-10} cm^2/W with both $W_{\mathrm{FOM}} = 1.02$ and $T_{\mathrm{FOM}} = 0.14$. Compared with multilayer graphene, Si, and GaAs, RPP ($I_{n=4}$) performs even better, as its nonlinear refractive index is enhanced by two orders of magnitude, while T_{FOM} is comparable [45,46]. Though RPPs ($I_{n=1,2,3}$) exhibit better T_{FOM} (<0.1), indicating less 2PA losses, the W_{FOM} values are less than 1 [29]. Note that the required light irradiance ($I = 10$ GW/cm^2) would be high. To reduce it, 2D materials in microcavities or photonic structures should be considered. For example, one may integrate 2D materials on clad nanophotonic cavities, such as ring and disk resonators, to increase the effective path length for light–matter interaction [47]. Arbitrary vertical heterostructures such as intentionally designed sequences of graphene, h-BN, and TMD monolayers (or 2D perovskites) [48,49] would give also rise to higher 2D-exciton density in order to reduce the operating light intensity.

Table 1. Nonlinear Coefficients and FOMs of Materials at 1550 nm

Material	n_2 [$\times 10^{-12}$ cm^2/W]	β [cm/GW]	W_{FOM}	T_{FOM}	Ref.
2D RPP ($I_{n=4}$)	105.5	96.3	1.02	0.14	This work
2D RPP ($I_{n=3}$)	22.9	9.9	0.27	0.07	This work
2D RPP ($I_{n=2}$)	7.2	1.6	0.12	0.03	This work
2D RPP ($I_{n=1}$)	1.3	0.3	0.03	0.04	This work
2D MoS_2	1.5	5.6	0.008	0.56	This work
2D $MoSe_2$	19.1	212.5	0.07	1.72	This work
2D WS_2	2.7	7.7	0.02	0.45	This work
2D WSe_2	15.8	79.1	0.06	0.78	This work
Multilayer graphene	−800	900	0.20	1.40	[37]
Si⟨110⟩	0.045	0.79	–	0.37	[45]
GaAs	0.16	10.2	–	0.10	[45]
GaAs/AlAs superlattice	0.15	1.5	–	0.87	[46]
Conjugated 3,3'-bipyridine derivative	0.0046	<0.01	>600	<0.15	[43]

4. CONCLUSION

In summary, based on the K-K transformation of exciton-associated 2PA, we have successfully developed an admirably succinct model to predict the OKE of 2D semiconductors. In our model, all the parameters are measurable experimentally, except for the linewidth of 2p exciton. On the examining the 10 2D materials mentioned here, we find that our model can provide a general guideline on both the n_2 magnitude and n_2 spectra. On our analysis, two-photon resonance with 2D excitons yields a remarkable contribution to the nonlinear refractive index spectra. As compared with the TPB model for 3D semiconductors, the OKE induced by 2D excitons shows a great enhancement. Based on this simple model, we assess RPP ($I_{n=4}$) crystals to be the best material candidate for all-optical switching at the 1550 nm wavelength. Our findings deepen the understanding of the OKE of 2D semiconducting materials and pave the way for highly efficient all-optical excitonic devices.

APPENDIX A: DERIVATION OF n_2 DISPERSION FOR 2D SEMICONDUCTORS WITH TWO EXCITONS

In monolayer transition metal dichalcogenides (TMDs), there are two distinctive excitons: exciton A and exciton B. For these 2D semiconductors with the two-exciton feature, by a quantum perturbation theory associated with 2D excitons, we have derived the wavelength-dependent, degenerate 2PA coefficient as [28]

$$\beta(\hbar\upsilon') = CN\hbar\upsilon'\left(\frac{E_{\mathrm{loc}}}{E}\right)^4 \times \left[\frac{|\mu_{G\to 1s}|^2}{(E_{1s\_A}-\hbar\upsilon')^2+(\Gamma_{1s\_A}/2)^2} + \frac{|\mu_{G\to 1s}|^2}{(E_{1s\_B}-\hbar\upsilon')^2+(\Gamma_{1s\_B}/2)^2}\right] \times \frac{|W_n\mu_{1s\to np}|^2\Gamma_{np}/2\pi}{(E_{np}-2\hbar\upsilon')^2+(\Gamma_{np}/2)^2}, \tag{A1}$$

where N is the density of active unit cells; $\frac{E_{\mathrm{loc}}}{E} = \frac{1}{3}(n_0^2+2)$ is the local-field correction factor; n_0 is the refractive index; $\hbar\upsilon'$ is the photon energy; E_{1s_A}, E_{1s_B}, and E_{np} are the energy level of the lowest 1s excitons (A exciton and B exciton) and higher np excitons, respectively. Γ_{1s_A}, Γ_{1s_B}, and Γ_{np} refer to their linewidth. $\mu_{i\to j}$ is the corresponding transition dipole moment from an i state to a j state. W_n is the weight value of an excitonic state; and C has a value of 3.47×10^{45} in units such that β is in cm/MW, N is in cm^{-3}, $\hbar\upsilon$, E_i, and Γ_i are in units of eV, and $\mu_{i\to j}$ is in units of esu. Both the transition dipole moments and the weight values can be obtained in Refs. [28,29].

Here, we assume that 1s- and np-excitonic states at room temperature have the equal linewidths, respectively ($\Gamma_{1s\_A} = \Gamma_{np\_A} = 2\hbar\gamma_A$, $\Gamma_{1s\_B} = \Gamma_{np\_B} = 2\hbar\gamma_B$). To fulfill the odd-parity requirement of two-photon transitions [50], only 2p excitons make the significant contribution to the 2PA ($E_{2p} \approx 2\hbar\upsilon'$), and other np-excitonic states are neglected, as shown in Table 2.

The 2PA coefficient from Eq. (A1) becomes

$$\beta(\hbar\upsilon') = \frac{CN(\hbar\gamma)}{81\pi}|W_2|^2|\mu_{G\to 1s}|^2|\mu_{1s\to 2p}|^2(n_0^2+2)^4 \times \left[\frac{1}{(E_{1s\_A}-\hbar\upsilon')^2+(\hbar\gamma_A)^2}\frac{\hbar\upsilon'}{(2\hbar\upsilon'-E_{2p\_A})^2+(\hbar\gamma_A)^2} + \frac{1}{(E_{1s\_B}-\hbar\upsilon')^2+(\hbar\gamma_B)^2}\frac{\hbar\upsilon'}{(2\hbar\upsilon'-E_{2p\_B})^2+(\hbar\gamma_B)^2}\right], \tag{A2}$$

where the energy of 2p-excitonic state (E_{2p}) is replaced with E_{2p_A} and E_{2p_B}. With approximations that $|E_{1s}-\hbar\upsilon'| \gg \hbar\gamma$ and $E_{1s} \approx E_{2p} \gg \hbar\upsilon'$, Eq. (A2) is simplified to be

Table 2. Normalized Transition Dipole Moments for 2PA Transitions[a]

2PA Transitions	$\lvert\mu_{G\to 1s}\rvert\lvert\mu_{1s\to np}\rvert$ [a.u.]
G → 1s → 2p	1
G → 1s → 2s	0
G → 1s → 3p	0.41
G → 1s → 3s	0
G → 1s → 4p	0.24
G → 1s → 5p	0.16
G → 1s → 6p	0.11

[a]Note: Transition dipole moments are normalized by $|\mu_{G\to 1s}||\mu_{1s\to 2p}|$ amplitude [28].

$$\beta(\hbar\upsilon') = \frac{CN(\hbar\gamma)}{81\pi}|W_2|^2|\mu_{G\to 1s}|^2|\mu_{1s\to 2p}|^2(n_0^2+2)^4 \times\left[\frac{1}{E_{2p\_A}^2}\frac{\hbar\upsilon'}{(2\hbar\upsilon'-E_{2p\_A})^2+(\hbar\gamma_A)^2} + \frac{1}{E_{2p\_B}^2}\frac{\hbar\upsilon'}{(2\hbar\upsilon'-E_{2p\_B})^2+(\hbar\gamma_B)^2}\right]. \tag{A3}$$

By substituting Eq. (A3) into the K-K transformation, the n_2 dispersion is derived to be

$$n_2(\hbar\upsilon) = \frac{CN(c\hbar^2\gamma)}{81\pi^2}|W_2|^2|\mu_{G\to 1s}|^2|\mu_{1s\to 2p}|^2(n_0^2+2)^4 \times\int_{-\infty}^{+\infty}\left[\frac{1/E_{2p\_A}^2}{(2\hbar\upsilon'-E_{2p\_A})^2+(\hbar\gamma_A)^2} + \frac{1/E_{2p\_B}^2}{(2\hbar\upsilon'-E_{2p\_B})^2+(\hbar\gamma_B)^2}\right]\times\frac{\hbar\upsilon'}{(\hbar\upsilon')^2-(\hbar\upsilon)^2}\mathrm{d}(\hbar\upsilon'). \tag{A4}$$

Because the equivalence of $\hbar\upsilon$ and $\hbar\upsilon'$ would lead to the integral of $\beta(\hbar\upsilon')$ with infrared divergences, a substitution of υ' with $\upsilon'+\Delta\upsilon'$ and a numerical summation were made for an approximate integral of β over the 2PA range $(0<\hbar\upsilon'<E_{2p})$. With further simplifications, we obtain a semi-empirical expression for n_2 as

$$n_2(\hbar\upsilon) = \frac{Z_2'(n_0^2+2)^4}{E_{2p}^2}[G_A(x)+G_B(x)], \tag{A5}$$

$$G_A(x) = \frac{0.5-x}{(0.5-x)^2+0.3(\hbar\gamma/E_{2p})^2}, \tag{A6}$$

and

$$G_B(x) = \frac{\Lambda\delta^2(1-0.5\delta-x)}{(1-0.5\delta-x)^2+0.3\delta^2(\Lambda\hbar\gamma/E_{2p})^2}. \tag{A7}$$

Here, $x=\frac{\hbar\upsilon}{E_{2p}}$. $\delta = E_{2p\_A}/E_{2p\_B}$ denotes an energy deviation of the spin-orbital splitting. $\Lambda=\hbar\gamma_B/\hbar\gamma_A$ is the ratio of linewidths of the split excitons [51,52] with $\hbar\gamma=\hbar\gamma_A$ being the best fitting parameter of A excitons. $Z_2' = C'N|\mu_{G\to 1s}|^2\cdot|\mu_{1s\to 2p}|^2(\hbar\gamma)\propto D_e a_B^4(\hbar\gamma)$ refers to a material-related parameter, where D_e and a_B are the density and the Bohr radius of the 2D exciton, respectively. As for the 10 2D materials listed in Table 3, one may calculate the Z_2' values and find that they are in the range from 0.98×10^{-15} to 1.67×10^{-15} with an average value of 1×10^{-14}, in the units such that n_2 is in cm^2/W; $\hbar\upsilon$, E_{2p}, and $\hbar\gamma$ are in units of eV. E_{2p} in Eq. (A5) interprets the energy of the A exciton at the $2p$ state, which is given by $E_{2p}\approx E_g - E_b/n_0^2 - 0.1$. E_b is the exciton binding energy. All parameters used in the calculation of n_2 dispersions are listed in Table 3.

APPENDIX B: SIMPLIFICATION OF n_2 DISPERSION OF 2D SEMICONDUCTORS WITH ONE EXCITON

For 2D materials without the spin-orbital splitting, the 2PA coefficient from Eq. (A3) becomes

$$\beta(\hbar\upsilon') = \frac{CN(c\hbar^2\gamma)}{81\pi^2}|W_2|^2|\mu_{G\to 1s}|^2|\mu_{1s\to 2p}|^2 \times\frac{(n_0^2+2)^4}{E_{2p}^2}\frac{\hbar\upsilon'}{(2\hbar\upsilon'-E_{2p})^2+(\hbar\gamma)^2}. \tag{B1}$$

Here, we define a parameter $C_2=\frac{CN(\hbar\gamma)}{81\pi}|W_2|^2|\mu_{G\to 1s}|^2\cdot|\mu_{1s\to 2p}|^2$ for the simplification of the 2PA coefficient. By substituting Eq. (B1) into the K-K transformation, the n_2 dispersion of 2D semiconductors with one exciton can be obtained. Furthermore, we have $\delta = E_{2p\_A}/E_{2p\_B}=1$ when there is no spin-orbital splitting of 2D materials. Equation (A5) can be simplified to be

$$n_2(\hbar\upsilon) = \frac{Z_2'(n_0^2+2)^4}{E_{2p}^2}G(x), \tag{B2}$$

where $G_A(x)=G_B(x)=G(x)$ becomes

$$G(x) = \frac{0.5-x}{(0.5-x)^2+0.3(\hbar\gamma/E_{2p})^2}. \tag{B3}$$

Equation (B2) is used to calculate the n_2 dispersions of 2D RPPs, h-BN, and BP.

Table 3. Parameters Used in the Calculation of n_2 Dispersions[a]

	n_0	a_B [Å]	D_e	E_g [eV]	E_b [eV]	E_{1s} [eV]	E_{2p} [eV]	Z_2' [$\times10^{-15}$]	$\hbar\gamma$ [eV]	δ	Λ
RPP ($I_{n=1}$)	2.11	15.3	0.60×10^{20}	2.74	0.35	2.39	2.59	0.979	0.15	N.A.	N.A.
RPP ($I_{n=2}$)	2.21	17.1	1.20×10^{20}	2.51	0.26	2.25	2.37	3.05	0.15	N.A.	N.A.
RPP ($I_{n=3}$)	2.27	17.9	1.80×10^{20}	2.27	0.16	2.11	2.14	5.50	0.15	N.A.	N.A.
RPP ($I_{n=4}$)	2.32	22.0	2.40×10^{20}	2.14	0.15	1.99	2.00	16.7	0.15	N.A.	N.A.
MoS_2	1.84	9.3	5.00×10^{20}	2.70	0.80	1.90	2.50	1.67	0.075	0.939	2
$MoSe_2$	2.10	10.1	1.81×10^{21}	2.43	0.66	1.77	2.21	8.40	0.075	0.909	2
WS_2	1.82	10.3	6.28×10^{20}	2.92	0.82	2.10	2.73	3.17	0.075	0.867	4
WSe_2	1.84	10.5	2.28×10^{21}	2.57	0.79	1.78	2.35	12.4	0.075	0.848	4
h-BN	2.00	6.1	2.40×10^{21}	5.81	0.92	5.50	5.69	1.00	0.15	N.A.	N.A.
BP	2.50	20.2	3.80×10^{20}	1.60	0.50	1.10	1.20	20.0	0.15	N.A.	N.A.

[a]Note that no fitting parameter was used in plotting the theoretical curves, except for the linewidth, and the experimental data of n_2 values [14,15,28,29,53–55] are scaled with the average value of $Z_2'=1\times10^{-14}$.

APPENDIX C: EXPERIMENTAL DATA OF n_2 VALUES

Table 4. Extracted n_2 Values from Experimental Data

	n_2 [$\times 10^{-12}$ cm^2/W]	$\frac{n_2 E_{2p}^2}{Z_2'(n_0^2+2)^4}$	λ [nm]	n_0	Ref.
RPP ($I_{n=1}$)	0.41	0.16	2700	2.11	[25]
RPP ($I_{n=2}$)	0.45	0.11	2700	2.21	[25]
RPP ($I_{n=3}$)	0.39	0.048	2700	2.41	[25]
RPP ($I_{n=4}$)	0.40	0.053	2700	2.32	[25]
MoS_2	−1.96	−1.45	800	1.84	[30]
	350	260.02	800	1.84	[38]
	1.88	1.40	1064	1.84	[38]
	−0.21	−0.15	1064	1.84	[31]
$MoSe_2$	−0.12	−0.034	1064	2.10	[31]
	0.20	0.058	1000	2.10	[39]
WS_2	−1.10	−1.02	800	1.82.	[30]
	0.81	0.76	800	1.82	[32]
	58.30	54.55	1064	1.82	[40]
	128	119.77	1040	1.82	[41]
WSe_2	−18.70	−12.27	1040	1.84	[41]
h-BN	0.12	0.30	1064	2.0	[33]
BP	860	26.73	800	2.5	[34]

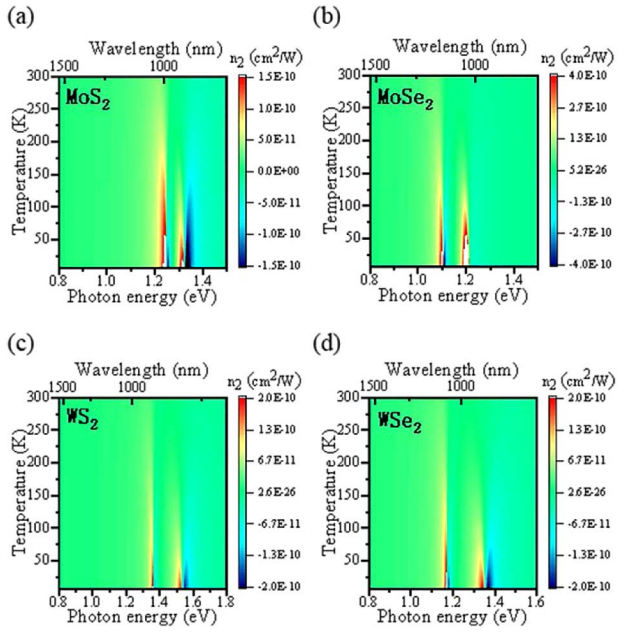

Fig. 7. Nonlinear refractive index, n_2, as a function of photon energy (x axis) and temperature (y axis) for TMD monolayers: (a) MoS_2, (b) $MoSe_2$, (c) WS_2, and (d) WSe_2. These n_2 values are calculated with the averaged $Z_2' = 1 \times 10^{-14}$.

APPENDIX D: TEMPERATURE DEPENDENCE OF NONLINEAR REFRACTIVE INDEX

According to Eq. (4) or (6), n_2 values are predicted to have the linewidth dependence in the near-resonance region in our model. Previous work [42] has demonstrated experimentally that the temperature-dependent linewidth of exciton absorption in perovskites can be expressed empirically by

$$\gamma(T) = \frac{\Gamma_0 + \sigma T + \Gamma_{LO}(e^{\hbar\omega_{LO}/k_B T} - 1)^{-1}}{2\hbar}, \quad \textbf{(D1)}$$

where Γ_0 is a temperature-independent inhomogeneous broadening term, which is determined by the material size, shape,

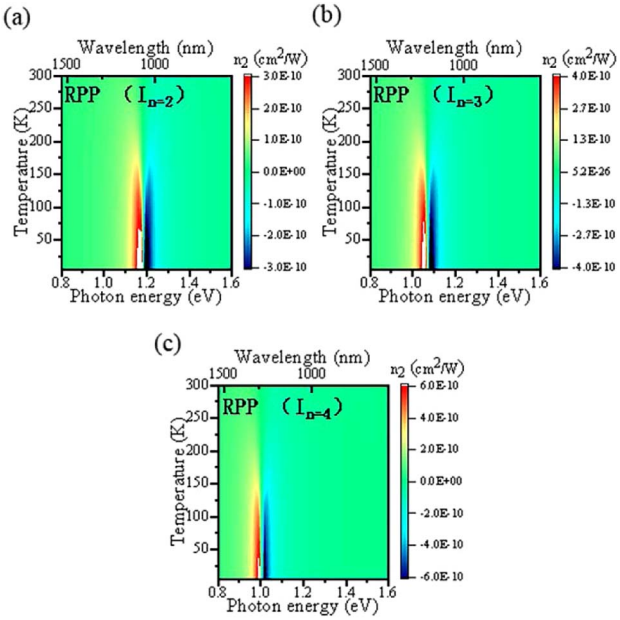

Fig. 6. Nonlinear refractive index, n_2, as a function of photon energy (x axis) and temperature (y axis) for monolayer RPP: (a) $I_{n=2}$, (b) $I_{n=3}$, and (c) $I_{n=4}$. These n_2 values are calculated with the averaged $Z_2' = 1 \times 10^{-14}$.

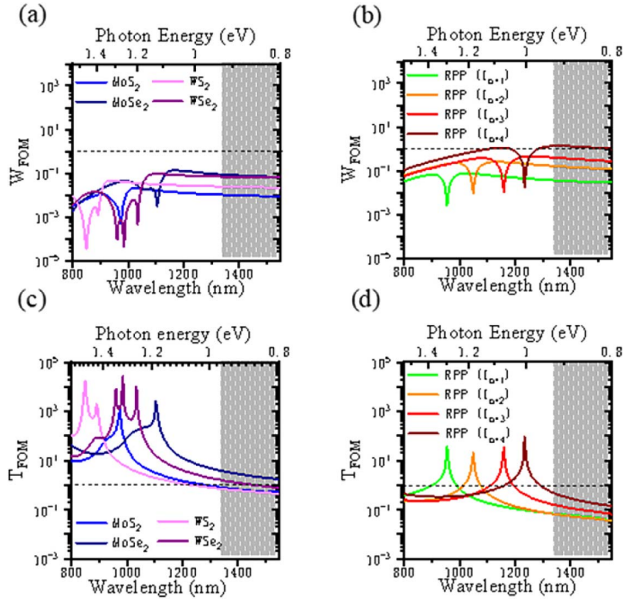

Fig. 8. (a) W_{FOM} of monolayer TMDs, (b) W_{FOM} of monolayer RPPs, (c) T_{FOM} of monolayer TMDs, and (d) T_{FOM} of monolayer RPPs. The gray area corresponds to the wavelength range for optical communications.

and composition; σ represents the coupling strength of acoustic phonon scattering; and Γ_{LO} represents the coupling strength of optical (LO) phonon scattering, which has a Bose–Einstein distribution for occupation numbers of the respective LO phonons. Here, for computation ease, the linewidths of the RPPs ($I_{n=1,2,3,4}$) or TMDs are assumed to be the same, as the variations among these 2D materials are insignificant. As a result, temperature dependence of n_2 dispersion of RPPs ($I_{n=1,2,3,4}$) and TMDs can be calculated and displayed in Figs. 5(a), 6, and 7.

APPENDIX E: FIGURES OF MERIT OF MONOLAYER RPPS AND TMDS

To evaluate the OKE efficiency for all-optical switching devices, we have calculated the figures of merit (FOMs) for monolayer RPPs and TMDs in the wavelength range from 600 to 1700 nm. Results are displayed in Fig. 8. The W_{FOM} values were calculated with $I_0 = 10\ W/cm^2$, the maximum peak intensity before the onset of irreversible change or damage in the material [28,29], which represents the maximum nonlinear phase shift that can be achieved with the material. In the transparent spectral region, α_0 is estimated to be $2 \times 10^6\ cm^{-1}$ for RPPs [56]; and $1.4 \times 10^5\ cm^{-1}$ for monolayer TMDs [57], respectively.

Funding. National University of Singapore and Ministry of Education of the Singapore government (R-144-000-401-114, R-144-000-445-114); China Postdoctoral Science Foundation (2020M672763); Science and Technology Innovation Commission of Shenzhen (JCYJ20170302153323978, JCYJ20170410171958839); Education Commission of Guangdong Province (2016KCXTD006).

Disclosures. The authors declare no conflicts of interest.

Data Availability. Data underlying the results presented in this paper are not publicly available at this time but may be obtained from the authors upon reasonable request.

REFERENCES

1. R. W. Boyd, *Nonlinear Optics* (Academic, 2020).
2. A. Newell, *Nonlinear Optics* (CRC Press, 2018).
3. X. Hu, P. Jiang, C. Ding, H. Yang, and Q. Gong, "Picosecond and low-power all-optical switching based on an organic photonic-bandgap microcavity," Nat. Photonics **2**, 185–189 (2008).
4. L. Deng, E. W. Hagley, J. Wen, M. Trippenbach, Y. Band, P. S. Julienne, J. E. Simsarian, K. Helmerson, S. L. Rolston, and W. D. Phillips, "Four-wave mixing with matter waves," Nature **398**, 218–220 (1999).
5. K. Inoue, T. Mukai, and T. Saitoh, "Nearly degenerate four-wave mixing in a traveling-wave semiconductor laser amplifier," Appl. Phys. Lett. **51**, 1051–1053 (1987).
6. K. J. A. Ooi, D. K. T. Ng, T. Wang, A. K. L. Chee, S. K. Ng, Q. Wang, L. K. Ang, A. M. Agarwal, L. C. Kimerling, and D. T. H. Tan, "Pushing the limits of CMOS optical parametric amplifiers with USRN: Si_7N_3 above the two-photon absorption edge," Nat. Commun. **8**, 13878 (2017).
7. T. Brabec, C. Spielmann, P. F. Curley, and F. Krausz, "Kerr lens mode locking," Opt. Lett. **17**, 1292–1294 (1992).
8. X. Liu, D. Popa, and N. Akhmediev, "Revealing the transition dynamics from Q switching to mode locking in a soliton laser," Phys. Rev. Lett. **123**, 093901 (2019).
9. M. J. Weber, D. Milam, and W. L. Smith, "Nonlinear refractive index of glasses and crystals," Opt. Eng. **17**, 175463 (1978).
10. R. Adair, L. L. Chase, and S. A. Payne, "Nonlinear refractive index of optical crystals," Phys. Rev. B **39**, 3337–3350 (1989).
11. X. J. Zhang, W. Ji, and S. H. Tang, "Determination of optical nonlinearities and carrier lifetime in ZnO," J. Opt. Soc. Am. B **14**, 1951–1955 (1997).
12. M. Sheik-Bahae, D. J. Hagan, and E. W. Van Stryland, "Dispersion and band-gap scaling of the electronic Kerr effect in solids associated with two-photon absorption," Phys. Rev. Lett. **65**, 96–99 (1990).
13. T. Olsen, S. Latini, F. Rasmussen, and K. S. Thygesen, "Simple screened hydrogen model of excitons in two-dimensional materials," Phys. Rev. Lett. **116**, 056401 (2016).
14. G. Zhang, A. Chaves, S. Huang, F. Wang, Q. Xing, T. Low, and H. Yan, "Determination of layer-dependent exciton binding energies in few-layer black phosphorus," Sci. Adv. **4**, 9977 (2018).
15. B. Arnaud, S. Lebègue, P. Rabiller, and M. Alouani, "Huge excitonic effects in layered hexagonal boron nitride," Phys. Rev. Lett. **96**, 026402 (2006).
16. Z. Jiang, Z. Liu, Y. Li, and W. Duan, "Scaling universality between band gap and exciton binding energy of two-dimensional semiconductors," Phys. Rev. Lett. **118**, 266401 (2017).
17. K. F. Mak, D. Xiao, and J. Shan, "Light–valley interactions in 2D semiconductors," Nat. Photonics **12**, 451–460 (2018).
18. C. Trovatello, F. Katsch, N. J. Borys, M. Selig, K. Yao, R. Borrego-Varillas, F. Scotognella, I. Kriegel, A. Yan, A. Zettl, P. J. Schuck, A. Knorr, G. Cerullo, and S. Dal Conte, "The ultrafast onset of exciton formation in 2D semiconductors," Nat. Commun. **11**, 5277 (2020).
19. A. Autere, H. Jussila, Y. Dai, Y. Wang, H. Lipsanen, and Z. Sun, "Nonlinear optics: nonlinear optics with 2D layered materials," Adv. Mater. **30**, 1870172 (2018).
20. I. Abdelwahab, P. Dichtl, G. Grinblat, K. Leng, X. Chi, I.-H. Park, M. P. Nielsen, R. F. Oulton, K. P. Loh, and S. A. Maier, "Giant and tunable optical nonlinearity in single-crystalline 2D Perovskites due to excitonic and plasma effects," Adv. Mater. **31**, 1902685 (2019).
21. N. Dong, Y. Li, S. Zhang, N. McEvoy, R. Gatensby, G. S. Duesberg, and J. Wang, "Saturation of two-photon absorption in layered transition metal dichalcogenides: experiment and theory," ACS Photon. **5**, 1558–1565 (2018).
22. Y. Yu, Y. Yu, C. Xu, A. Barrette, K. Gundogdu, and L. Cao, "Fundamental limits of exciton-exciton annihilation for light emission in transition metal dichalcogenide monolayers," Phys. Rev. B **93**, 201111 (2016).
23. A. Tanaka, N. J. Watkins, and Y. Gao, "Hot-electron relaxation in the layered semiconductor 2H-MoS_2 studied by time-resolved two-photon photoemission spectroscopy," Phys. Rev. B **67**, 113315 (2003).
24. H. H. Fang, J. Yang, S. Adjokatse, E. Tekelenburg, M. E. Kamminga, H. Duim, J. Ye, G. R. Blake, J. Even, and M. A. Loi, "Band-edge exciton fine structure and exciton recombination dynamics in single crystals of layered hybrid perovskites," Adv. Funct. Mater. **30**, 1907979 (2020).
25. F. O. Saouma, C. C. Stoumpos, J. Wong, M. G. Kanatzidis, and J. I. Jang, "Selective enhancement of optical nonlinearity in two-dimensional organic-inorganic lead iodide perovskites," Nat. Commun. **8**, 742 (2017).
26. B. Guo, Q. L. Xiao, S. H. Wang, and H. Zhang, "2D layered materials: synthesis, nonlinear optical properties, and device applications," Laser Photon. Rev. **13**, 1800327 (2019).
27. G. Grinblat, I. Abdelwahab, M. P. Nielsen, P. Dichtl, K. Leng, R. F. Oulton, K. P. Loh, and S. A. Maier, "Ultrafast all-optical modulation in 2D hybrid perovskites," ACS Nano **13**, 9504–9510 (2019).
28. F. Zhou, J. H. Kua, S. Lu, and W. Ji, "Two-photon absorption arises from two-dimensional excitons," Opt. Express **26**, 16093–16101 (2018).
29. F. Zhou, I. Abdelwahab, K. Leng, K. P. Loh, and W. Ji, "2D perovskites with giant excitonic optical nonlinearities for high-performance sub-bandgap photodetection," Adv. Mater. **31**, 1904155 (2019).

30. T. Neupane, B. Tabibi, and F. J. Seo, "Spatial self-phase modulation in WS_2 and MoS_2 atomic layers," Opt. Mater. Express **10**, 831–842 (2020).
31. K. Wang, Y. Feng, C. Chang, J. Zhan, C. Wang, Q. Zhao, J. N. Coleman, L. Zhang, W. J. Blau, and J. Wang, "Broadband ultrafast nonlinear absorption and nonlinear refraction of layered molybdenum dichalcogenide semiconductors," Nanoscale **6**, 10530–10535 (2014).
32. X. Zheng, Y. Zhang, R. Chen, Z. Xu, and T. Jiang, "Z-scan measurement of the nonlinear refractive index of monolayer WS_2," Opt. Express **23**, 15616–15623 (2015).
33. P. Kumbhakar, A. K. Kole, C. S. Tiwary, S. Biswas, S. Vinod, J. Taha-Tijerina, U. Chatterjee, and P. M. Ajayan, "Nonlinear optical properties and temperature-dependent UV-vis absorption and photoluminescence emission in 2D hexagonal boron nitride nanosheets," Adv. Opt. Mater. **3**, 828–835 (2015).
34. X. Zheng, R. Chen, G. Shi, J. Zhang, Z. Xu, and T. Jiang, "Characterization of nonlinear properties of black phosphorus nanoplatelets with femtosecond pulsed Z-scan measurements," Opt. Lett. **40**, 3480–3483 (2015).
35. T. C. Berkelbach, M. S. Hybertsen, and D. R. Reichman, "Theory of neutral and charged excitons in monolayer transition metal dichalcogenides," Phys. Rev. B **88**, 045318 (2013).
36. J. Wang, A. Coillet, O. Demichel, Z. Wang, D. Rego, A. Bouhelier, P. Grelu, and B. Cluzel, "Saturable plasmonic metasurfaces for laser mode locking," Light Sci. Appl. **9**, 50 (2020).
37. G. Demetriou, H. T. Bookey, F. Biancalana, E. Abraham, Y. Wang, W. Ji, and A. K. Kar, "Nonlinear optical properties of multilayer graphene in the infrared," Opt. Express **24**, 13033–13043 (2016).
38. F. Liu, X. Zhao, X. Q. Yan, X. Xin, Z. B. Liu, and J. G. Tian, "Measuring third-order susceptibility tensor elements of monolayer MoS_2 using the optical Kerr effect method," Appl. Phys. Lett. **113**, 051901 (2018).
39. H. Pan, H. Chu, Y. Li, S. Zhao, and D. Li, "Comprehensive study on the nonlinear optical properties of few-layered $MoSe_2$ nanosheets at 1 μm," J. Alloys Compd. **806**, 52–57 (2019).
40. S. Bikorimana, P. Lama, A. Walser, R. Dorsinville, S. Anghel, A. Mitioglu, A. Micu, and L. Kulyuk, "Nonlinear optical responses in two-dimensional transition metal dichalcogenide multilayer: WS_2, WSe_2, MoS_2 and $Mo_{0.5}W_{0.5}S_2$," Opt. Express **24**, 20685–20695 (2016).
41. N. Dong, Y. Li, S. Zhang, N. L. McEvoy, X. Zhang, Y. Cui, L. Zhang, G. S. Duesberg, and J. Wang, "Dispersion of nonlinear refractive index in layered WS_2 and WSe_2 semiconductor films induced by two-photon absorption," Opt. Lett. **41**, 3936–3939 (2016).
42. H. C. Woo, J. W. Choi, J. Shin, S. H. Chin, M. H. Ann, and C. L. Lee, "Temperature-dependent photoluminescence of $CH_3NH_3PbBr_3$ perovskite quantum dots and bulk counterparts," J. Phys. Chem. Lett. **9**, 4066–4074 (2018).
43. Q. Chen, E. H. Sargent, N. Leclerc, and A. J. Attias, "Wavelength dependence and figures of merit of ultrafast third-order optical nonlinearity of a conjugated 3, 3′-bipyridine derivative," Appl. Opt. **42**, 7235–7241 (2003).
44. F. Chérioux, A. J. Attias, and H. Maillotte, "Symmetric and asymmetric conjugated 3, 3′-bipyridine derivatives as a new class of third-order NLO chromophores with an enhanced non-resonant, nonlinear refractive index in the picosecond range," Adv. Funct. Mater. **12**, 203–208 (2002).
45. M. Dinu, F. Quochi, and H. Garcia, "Third-order nonlinearities in silicon at telecom wavelength," Appl. Phys. Lett. **82**, 2954–2956 (2003).
46. S. J. Wagner, J. Meier, A. S. Helmy, J. S. Aitchison, M. Sorel, and D. C. Hutchings, "Polarization-dependent nonlinear refraction and two-photon absorption in GaAs/AlAs superlattice waveguides below the half-bandgap," J. Opt. Soc. Am. B **24**, 1557–1563 (2007).
47. T. K. Fryett, A. Zhan, and A. Majumdar, "Phase-matched nonlinear optics via patterning layered materials," Opt. Lett. **42**, 3586–3589 (2017).
48. D. Pan, Y. Fu, N. Spitha, Y. Zhao, C. R. Roy, D. J. Morrow, D. D. Kohler, J. C. Wright, and S. Jin, "Deterministic fabrication of arbitrary vertical heterostructures of two-dimensional Ruddlesden-Popper halide perovskites," Nat. Nanotechnol. **16**, 159–165 (2021).
49. F. Withers, O. Del Pozo-Zamudio, A. Mishchenko, A. P. Rooney, A. Gholinia, K. Watanabe, T. Taniguchi, S. J. Haigh, A. K. Geim, A. I. Tartakovskii, and K. S. Novoselov, "Light-emitting diodes by band-structure engineering in van der Waals heterostructures," Nat. Mater. **14**, 301–306 (2015).
50. S. Uryu, H. Ajiki, and T. Ando, "Excitonic two-photon absorption in semiconducting carbon nanotubes within an effective-mass approximation," Phys. Rev. B **78**, 115414 (2008).
51. O. B. Aslan, M. Deng, and T. F. Heinz, "Strain tuning of excitons in monolayer WSe_2," Phys. Rev. B **98**, 115308 (2018).
52. E. Courtade, B. Han, S. Nakhaie, C. Robert, X. Marie, P. Renucci, T. Taniguchi, K. Watanabe, L. Geelhaar, J. M. J. Lopes, and B. Urbaszek, "Spectrally narrow exciton luminescence from monolayer MoS_2 and $MoSe_2$ exfoliated onto epitaxially grown hexagonal BN," Appl. Phys. Lett. **113**, 032106 (2018).
53. A. Segura, L. Artús, R. Cuscó, T. Taniguchi, G. Cassabois, and B. Gil, "Natural optical anisotropy of h-BN: highest giant birefringence in a bulk crystal through the mid-infrared to ultraviolet range," Phys. Rev. Mater. **2**, 024001 (2018).
54. T. C. Doan, J. Li, J. Y. Lin, and H. X. Jiang, "Bandgap and exciton binding energies of hexagonal boron nitride probed by photocurrent excitation spectroscopy," Appl. Phys. Lett. **109**, 122101 (2016).
55. X. Wang and S. Lan, "Optical properties of black phosphorus," Adv. Opt. Photon. **8**, 618–655 (2016).
56. I. Abdelwahab, G. Grinblat, K. Leng, Y. Li, X. Chi, A. Rusydi, S. A. Maier, and K. Ploh, "Highly enhanced third-harmonic generation in 2D perovskites at excitonic resonances," ACS Nano **12**, 644–650 (2018).
57. K. F. Mak, C. Lee, J. Hone, J. Shan, and T. F. Heinz, "Atomically thin MoS_2: a new direct-gap semiconductor," Phys. Rev. Lett. **105**, 136805 (2010).